nature communications

Article

https://doi.org/10.1038/s41467-024-54292-0

In vivo gene editing of T-cells in lymph nodes for enhanced cancer immunotherapy

Received: 7 March 2024

Accepted: 7 November 2024

Published online: 25 November 2024

Check for updates

Jin Qu[1,9], Yuan Wang[1,9], Chuxiao Xiong[1], Mingxue Wang[1], Xingdao He[1], Weibin Jia[1,2], Cheuk Yin Li[3], Tianlong Zhang[4], Zixun Wang[5], Wei Li[6], Becki Yi Kuang[3] & Peng Shi[1,2,7,8]

Immune checkpoint blockade (ICB) therapy, while promising for cancer treatment, faces challenges like unexpected side effects and limited objective responses. Here, we develop an in vivo gene-editing strategy for improving ICB cancer therapy in a lastingly effective manner. The approach uses a conductive hydrogel-based electroporation system to enable nucleofection of programmed cell death protein 1 (PD1) targeted CRISPR-Cas9 DNAs into T-cells directly within the lymph nodes, and subsequently produces PD1-deficient T-cells to combat tumor growth, metastasis and recurrence in different melanoma models in mice. Following in vivo gene editing, animals show enhanced cellular and humoral immune responses along with multi-fold increases of effector T-cells infiltration to the solid tumors, preventing tumor recurrence and prolonging their survival. These findings provide a proof-of-concept for direct in vivo T-cell engineering via localized gene-editing for enhanced cancer immunotherapy, and also unlock the possibilities of using this method to treat more complex human diseases.

Currently, surgery remains one of the major treatments for many cancer patients who suffer from solid tumors. Despite continuous improvements in surgical techniques, residual micro-tumors remain a significant problem for many patients. In many cases, the residual malignant tumor tissues are sufficient to cause lethal recurrence and metastasis[1]. Hence, tremendous efforts have been made to develop effective post-operative cancer treatments in recent years. Particularly, cancer immunotherapy shows great promises by harnessing the potency of the immune system as a therapeutic modality for cancer[2]. Among different technical routes of immunotherapy, ICB leads to durable clinical responses that have been verified by a fraction of cancer patients in long-term cancer remissions[3,4]. Instead of directly attacking particular targets on tumor cells, the goal of ICB therapy is to suppress the inhibitory pathways that block effective antitumor T-cell responses associated with the cytotoxic T lymphocyte-associated protein 4 (CTLA-4) or the programmed cell death 1 (PD1) pathway. Encouragingly, ICB provides an increased survival period and improved treatment effectiveness than platinum or paclitaxel-based chemotherapeutics, which are the most common choices in clinical practices[5]. ICB therapy also shows less toxicity than these traditional chemotherapies towards treating refractory cancer cases, making ICB an attractive therapy for improving quality of life beyond patients' survival[4,6].

Several chemical inhibitors targeting PD1 receptors (e.g., pembrolizumab, nivolumab) have been approved by the US Food and Drug

[1]Department of Biomedical Engineering, City University of Hong Kong, Kowloon, Hong Kong SAR, China. [2]Hong Kong Centre for Cerebro-Cardiovascular Health Engineering, Hong Kong Science Park, Hong Kong SAR, China. [3]Department of Chemical and Biological Engineering, The Hong Kong University of Science and Technology, Kowloon, Hong Kong SAR, China. [4]Department of Mechanical and Aerospace Engineering, The Hong Kong University of Science and Technology, Clear Water Bay, Hong Kong, China. [5]CAS Key Laboratory of Nano-Bio Interface, Suzhou Institute of Nano-Tech and Nano-Bionics, Chinese Academy of Sciences, Suzhou, China. [6]Department of Thyroid and Breast Surgery, Zhongnan Hospital of Wuhan University, School of Pharmaceutical Sciences, Wuhan University, Wuhan, China. [7]Center of Super-Diamond and Advanced Films (COSDAF), City University of Hong Kong, Kowloon, Hong Kong SAR, China. [8]Shenzhen Research Institute, City University of Hong Kong, Nanshan, Shenzhen, China. [9]These authors contributed equally: Jin Qu, Yuan Wang. e-mail: pengshi@cityu.edu.hk

Administration (FDA) for clinical use, but the development of refractoriness and drug resistance after a period of responsive treatment are still problematic[7–9]. Alternatively, intravenous infusion of therapeutic antibodies is limited by their systemic delivery approaches, causing off-target binding and unnecessary toxicities resulted from high doses[7,10,11]. Nuclease-based gene-editing systems can potentially expand the scope of ICB therapy by editing possible targets to block immune checkpoints in a lastingly effective manner[12], promising relatively low off-target blocking effect, a decrease in morbidity and cost of treatment, as well as improve patients' life quality without frequent drug administration[13,14]. Some studies have been done on the knockout or inhibition of PD1 in T-cells for the clearance of tumors in mice models. In many cases, the therapy involves ex vivo T-cells engineering and subsequent transplantation of engineered T-cell into diseased animals or patients. Two phase I clinical trials were conducted to evaluate the anti-cancer efficacy of CRISPR-Cas9 edited PD1-deficient T-cells[12,15].

Particularly, Lu and colleagues produced PD1-gene-edited bulk autologous T-cells for treating lung cancer in human patients with a CRISPR-Cas9 system. They isolated human peripheral blood mononuclear cells and transfected them via electroporation of DNA plasmids for deleting *PDCD1* (encoding PD1). The engineered T-cells were cultured before infusing into patients and are demonstrated with results supporting the feasibility and safety of gene editing for improved ICB therapy[15]. Carl et al. reported a human phase 1 clinical trial to manufacture CRISPR-Cas9 edited T-cells for refractory cancer, which also showed reasonable potency[12]. Nevertheless, a large number of engineered T-cells are typically needed for the aforementioned treatment strategies to be successful, which requires costly, complex, and labor-intensive ex vivo expansion of the therapeutic cells before they are infused into patients[13,16,17]. Very often, intravenous cell injection exhibits poor activity against solid tumors, as it is challenging for the cells to locate, infiltrate, and expand within the immunosuppressive tumor microenvironment (TME) following systemic administration[18,19]. Additionally, the lack of reliable quality control measures for ex vivo cell manufacturing also poses significant uncertainty for associated therapy[20,21]. Therefore, the capability to create engineered immune cells in vivo presents a broader range of possibilities for enhancing current immunotherapies, including ICB. Localized in vivo gene-editing in relevant organs and tissues promises a safe and efficient strategy, especially when the delivery of gene-editing reagent could be achieved in a footprint-free manner without relying on lipid nanoparticles or virus-based delivery systems.

In this study, we develop an in vivo gene edit strategy for improving ICB cancer therapy. The approach uses a conductive hydrogel-based electroporation system (hydro-EP) to enable nucleofection of PD1-targeted CRISPR-Cas9 DNAs into T lymphocytes directly within lymph node tissues, and subsequently produces engineered T-cells with suppressed PD1 to combat tumor growth, metastasis, and recurrence. In a melanoma rodent model, the engineered animals show multi-fold increase in the infiltration of PD1 deficient T-cells in solid tumors as a result of significantly enhanced cellular and humoral immune response, which further prolong the survival of tumor-bearing mice and eliminate the risk of tumor recurrence. Even in animals that receive a surgery to remove the primary tumor but still have a high metastasis potential, the gene-editing enhances ICB treatment, extends their survival span by multiple folds, and achieves a nearly complete alleviation in some mice. These findings provide a proof-of-concept of direct T-cell engineering in living animals by localized gene-editing within lymph node to enhance immune-cancer therapy, and also show the promise of employing in vivo gene editing to treat more complex diseases.

Results

Localized electroporation for producing CRISPR-Cas9-engineered T-cells in vivo

By leveraging conductive hydrogel electrodes as a DNA carrier and traffic accelerator, preloaded CRISPR-Cas9 DNAs could be electrically triggered to release from the hydrogel and then intracellularly transfected into contacting cells upon another series of electrical pulsing. To perform in vivo T-cell engineering in a minimally invasive format, a hydrogel-based bioelectronic surgical forceps device was developed in this study (Fig. 1). It consists of two electrodes assembly integrated on the edge of a surgical forcep for electroporating lymph node tissues. The device includes a hydrogel-based working electrode (hWE) and a metal ground electrode (mGE). The flexible hWE and mGE were mounted on the tip or the side of the forceps depending on different application (Fig. 1b, c, and Supplementary Figs. 1, 2). The hWE was designed to assume a microneedle structure, intended to breach the lymph node capsule and to access the T-cell enriched paracortical region at approximately 1 mm depth in a lymph node for maximized transfection of T-cells (Supplementary Figs. 3, 4, Supplementary Note 1). Because of the low working voltage and brief operation time, the mGE (copper-based) does not release any toxic Cu^{2+} into the contacting tissue (Supplementary Fig. 5). First, we evaluated the in vivo production of CRISPR-Cas9-edited PD1-deficient T-cells as a proof-of-concept. The T-cell remodeling in response to cancer development is evaluated in an established murine melanoma tumor model produced by subcutaneous injection of skin melanoma cells (B16F10). The tumor cells injection in C57BL/6 mice was performed five days ahead of treatment to ensure successful tumor establishment and proper T-cell activation, which is a common prerequisite of $PD1^+$ T-cell production[3]. PD1-deficient T-cells are produced by in-situ electroporation of the lymph node tissue for PD1-CRISPR-Cas9 plasmid to be delivered into the T lymphocytes via a two-stage procedure. In the first stage, using a long voltage stimulation (1 V, 20 min), the pre-loaded negative charged DNA plasmids were driven to release from the hWE via an electrophoresis-like process. The electrical trigger parameters, voltage amplitude and stimulation, were optimized to ensure efficient and safe release of DNAs from the hydro-EP device (Supplementary Fig. 6). In the second stage, a pulsed electric field was applied across the electrodes to transiently electroporate the exposed cells and for the NA cargo (PD1-CRISPR-Cas9 plasmids) to be directly transferred into the cell cytosol[22]. It was expected that the electroporation parameters, including voltage amplitude, pulsing frequency, width and pulse number, would have profound impact on the cellular transfection efficiency[23]. Before any in vivo experiments, a series of ex vivo characterizations were performed to derive the optimized pulsing parameters (90 V, 1 Hz, 50 ms pulse width, 10 pulses) for safe and efficient electroporation of human cells (Supplementary Fig. 7). 7 days after the in vivo electroporation surgery (Supplementary Fig. 8), the lymph nodes were collected and analyzed to evaluate the transgenic T-cell production (Fig. 2a). Supplementary Fig. 9 shows the details of PD1-CRISPR-Cas9 plasmid that was used in this study.

The success of DNA transfection in the lymph node was confirmed by the expression of eGFP plasmids delivered to the lymph node cells. Only 24 h after a treatment, the hydro-EP approach achieved the substantial eGFP expression ($15.3 \pm 2.4\%$), which showed a significant improvement over the lipofection ($5.4 \pm 0.5\%$) and bulk electroporation controls ($6.9 \pm 1.0\%$) (Fig. 2b, c). These observations underscore the efficacy of the hydro-EP technique, achieving superior transfection efficiency in lymphocytes compared to other in vivo transfection methods. Through a closer look at the transfected cell populations, we found that successfully transfected T-cell ($eGFP^+CD3^+$), B-cell ($eGFP^+CD19^+$), dendritic cells ($eGFP^+CD11c^+$), natural killer cells ($eGFP^+NK1.1^+$) cells, and other cells accounted for $11.8 \pm 1.9\%$,

https://doi.org/10.1038/s41467-024-54292-0

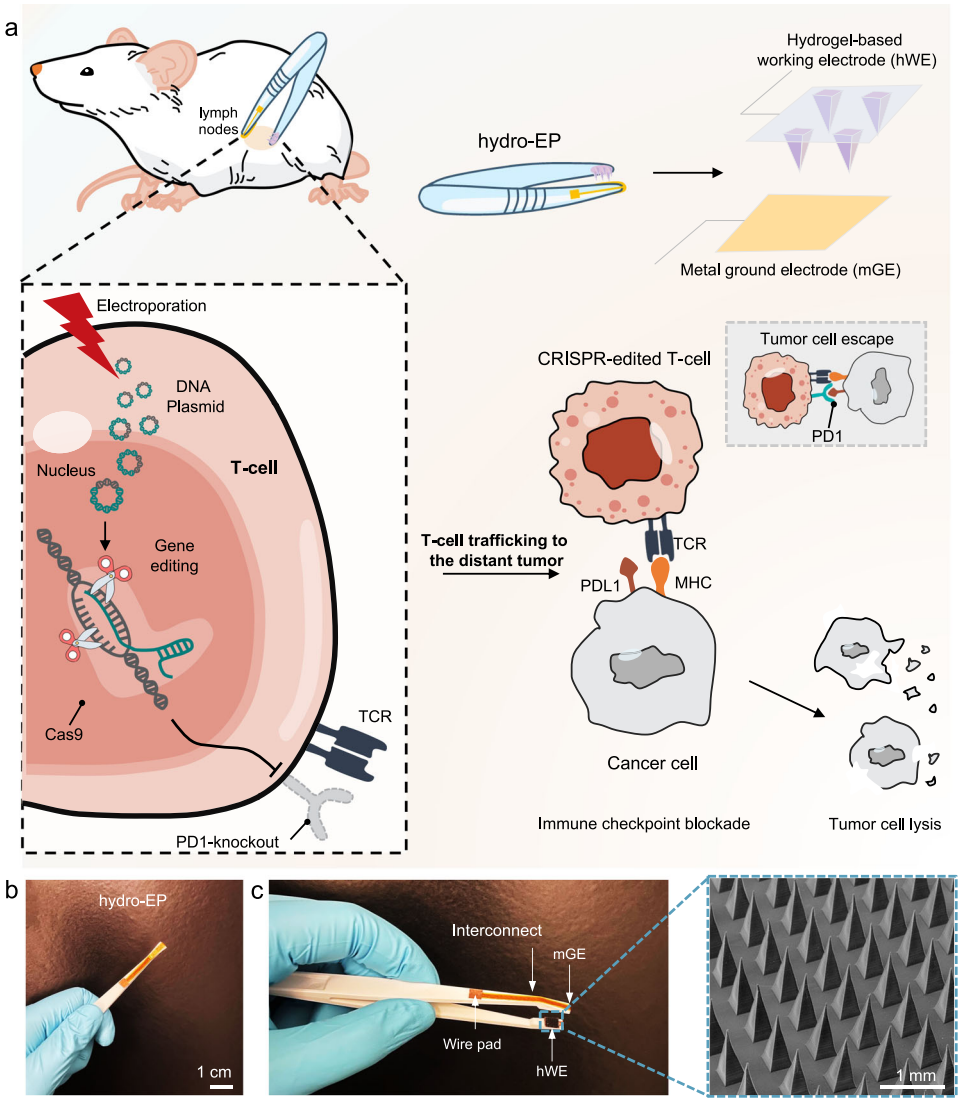

Fig. 1 | Schematic and characterization of in vivo T-cell engineering therapy. **a** Schematic of in vivo gene-editing in lymph node for localized T-cell engineering therapy through the conductive hydrogel-based electroporation system (hydro-EP) to enable nucleofection of PD1-targeted CRISPR-Cas9 DNAs into T lymphocytes directly within lymph node tissues, and subsequently produces engineered T-cells with suppressed PD1 to combat tumor growth, metastasis, and recurrence. TCR, T-cell receptor; MHC, major histocompatibility complex; PDL1, programmed death-ligand 1. **b** An overview photograph of a hydro-EP device. Scale bar, 1 cm. **c** A close-up photograph of the hydro-EP device, it consists of a hydrogel-based working electrode (hWE) and a metal-based ground electrode (mGE), that are assembly integrated on the edge of the surgical forceps for electroporating lymph node tissues. Inset: Representative SEM image of hWE with a microneedle structure loaded with PD1-CRISPR-Cas9 plasmids. Scale bar, 1 mm.

2.4 ± 0.5%, 0.7 ± 0.1%, 0.2 ± 0.05%, and 0.5 ± 0.3% of the whole cell population, respectively; the $CD3^+$ T-cells predominated (~75.6%) in all transfected cells (Fig. 2d). After the technical validation of in vivo transgenic engineering of T-cells in the lymph node, the expression of the functional DNA plasmid, PD1-CRISPR-Cas9, in the experimental mice were analyzed by immunofluorescence staining (IF) and flow cytometry (Fig. 2e–m), in order to verify the establishment of PD1-deficient activated T-cells in the lymph nodes via a focused in vivo electroporation. PD1 is typically not expressed in the lymph nodes of healthy animals, unless the T-cells are activated by the antigen-presenting cells (APCs) after tumor appearance[24]. Accordingly, substantially higher PD1 expression level was observed in the control tumor-bearing mice without any treatment (denoted as untreated group, Fig. 2e, f). With the in vivo local electroporation of PD1-CRISPR-Cas9 plasmids in the lymph node (denoted as PD1-CRISPR-Ele), the expression of PD1 in the lymph nodes cells was significantly suppressed (Fig. 2e, f), suggesting a success in the knockdown of PD1 by CRISPR-cas9 mediated gene editing, which could lead to elevated proliferation and activation of T-cells (Supplementary Fig. 10). Accordingly, it was not surprising to observe the increased percentage of $CD3^+CD4^+$ or $CD3^+CD8^+$ in the treated lymph node, and the break-up of $CD4^+$ and $CD8^+$ in the $CD3^+$ population remained similar for the hydro-EP or the untreated cases (Fig. 2g).

The flow cytometry analysis showed that there was a higher population of PD1 negative ($PD1^-$) cells (90.9%) in the PD1-CRISPR-Ele mice, while the proportion of $PD1^-$ cells was comparatively lower (78.9%) in untreated mice (Fig. 2h). Out of the $CD3^+$ T-cells, the $PD1^+$ subset was significantly lower in PD1-CRISPR-Ele animals, when compared to the untreated cases (Fig. 2i, 8.7 ± 0.8% vs. 17.2 ± 0.3%); however, the difference was not that evident for $CD3^-$ non-T-cell populations (Fig. 2i, 3.7 ± 0.4% vs. 5.5 ± 0.3%), suggesting that the local gene-editing mediated PD1 knockdown primarily affecting $CD3^+$ T-cells, which is consistent with our observation of the predominant DNA transfection in $CD3^+$ T-cells (Fig. 2d).

To evaluate the PD1 knockdown efficiency in the lymph nodes, from normal mice (no tumor inoculation), we extracted the lymph

https://doi.org/10.1038/s41467-024-54292-0

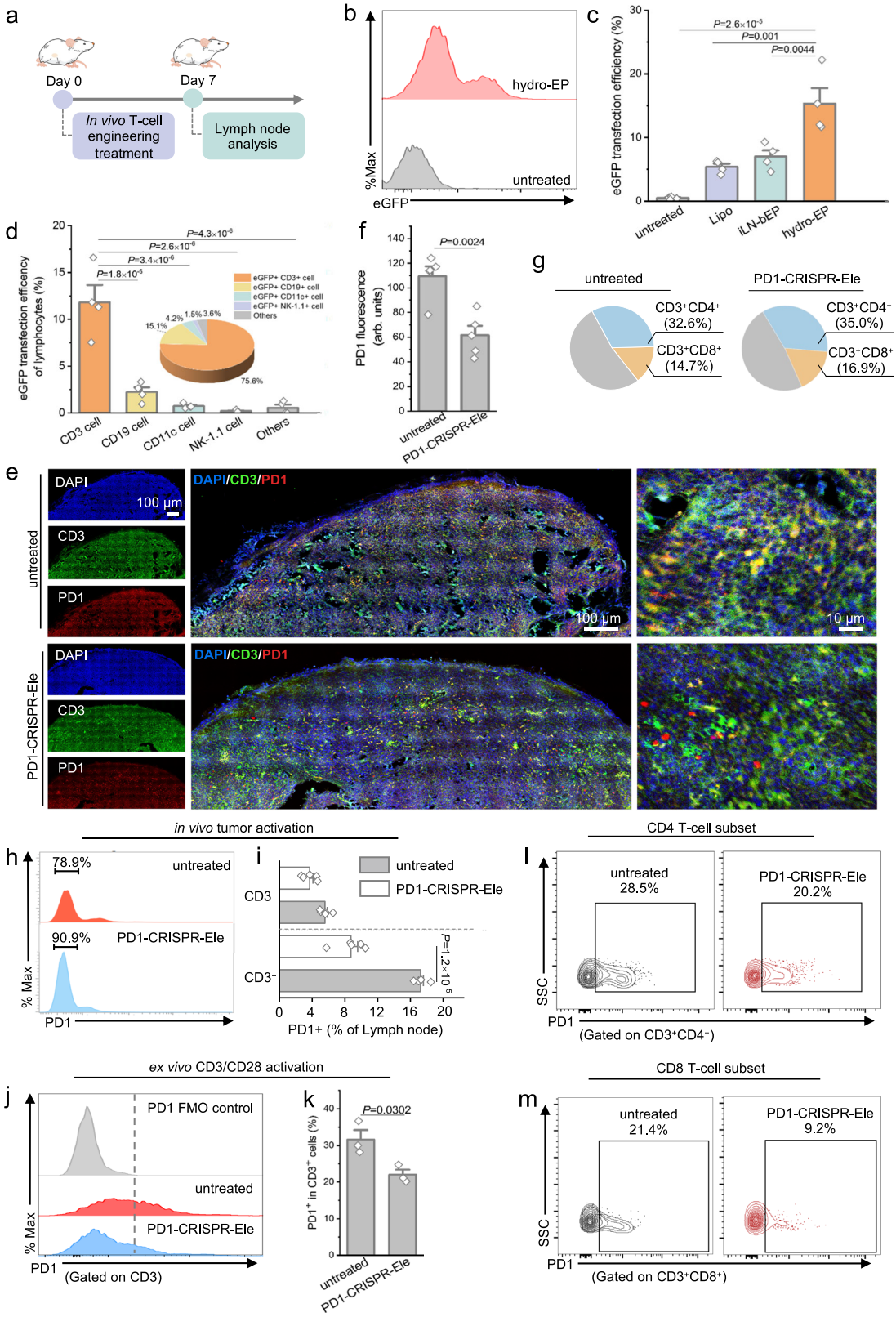

nodes 24 h after in vivo electroporation by hydro-EP, prepared single-cell suspension, and isolated T-cells ($CD3^+$), which should not express PD1 due to a lack of tumor antigen experience. The T-cells were then stimulated with CD3/CD28 T-cell activator. 48 h after CD3/CD28 co-stimulation, ~20% of the T-cells were tested to be PD1 positive for the animals received PD1 knockdown; while more than 30% of the T-cells were PD1 positive for the untreated animals (Fig. 2j, k). Accordingly, it was estimated that ~10% of the T-cells were successfully transfected and showed proper inhibition of PD1 expression. Next, we examined the $PD1^+$ cells in $CD4^+$ and $CD8^+$ lymphocytes. In the PD1-CRISPR-Ele group, the $CD4^+PD1^+$ cells were enriched at a percentage of 20.2%, which is significantly lower than

Fig. 2 | CRISPR-Cas9-engineered T-cells produced via a localized in vivo electroporation. a A one-time treatment of focused in vivo lymph node electroporation lasting several minutes led to PD1-deficient T-cell production (day 7) in a minimally invasive surgery manner. **b** Flow cytometry analysis and (**c**) quantification data showing eGFP plasmid DNA transfection efficiencies with different in vivo delivery methods. **d** The qualification of eGFP transfection in different types of lymph node cells. Insert: The proportion of different lymphocytes within the eGFP-positive population. For (**c**, **d**), $n = 4$ mice in each group. Fluorescence microscopy images (**e**) and fluorescence qualification (**f**) of lymph node slice after PD1-CRISPR-Ele treatment *versus* untreated group. Scale bar, 100 μm. Scale bar, 10 μm in enlarged view. $n = 5$ independent samples. **g** Quantification of finely classified different T lymphocytes subsets. **h** Lymphocytes were isolated from the lymph nodes of mice 7 days after PD1-CRISPR-Ele treatment. Representative flow cytometry analysis of PD1 negative ($PD1^-$) cells population upon PD1-CRISPR-Ele treated group and untreated group. **i** Quantification of the proportion of PD1 positive ($PD1^+$) cells in the $CD3^+$ (T-cells) and $CD3^-$ subsets (non-T-cells). $n = 5$ mice in each group. **j**, **k** Artificial ex vivo stimulation of lymph node cells (from healthy mice) to evaluate the PD1 knockdown efficiency. **j** Flow cytometry analysis and (**k**) qualification of PD1 expression in the $CD3^+$ T-cells after a manual activation using the CD3/CD28 T-cell activator, $n = 3$ mice in each group. Flow cytometric analysis of PD1 expression on $CD4^+$ T lymphocytes (**l**) and $CD8^+$ T lymphocytes (**m**) extracted from the lymph nodes of different groups, $n = 4$ mice in each group. The data are presented as mean ± s.e.m. Statistical significance was calculated by two-sided Student's *t* test for two group comparison, one-way ANOVA with Tukey's test for multiple comparisons. Source data are provided as a Source Data file.

what is observed in the untreated group (28.5%, Fig. 2l). Similar observation was also made for the $CD8^+PD1^+$ cells, which was compared at 9.2% (PD1-CRISPR-Ele) *vs.* 21.4% (untreated, Fig. 2m), emphasizing the success of gene-editing in the functional T-cells by in vivo transfection of PD1-CRISPR-Cas9 DNA plasmids. Later, the lymph nodes were collected and sliced for haematoxylin and eosin staining (H&E staining), which revealed that no obvious histological damage was induced by the hydro-EP treatment (Supplementary Fig. 4), suggesting the technique as a safe and convenient electroporation platform for localized cell engineering in vivo.

Systemic antitumor immunity induced by gene-edited T-cell

We next assessed the systemic antitumor effects elicited by the in vivo engineered T-cells, which were gene-edited to be PD1 negative. Before any treatments, B16F10 cells were implanted subcutaneously on the flank of the healthy C57BL/6 mice for five days. The tumor-bearing mice were treated with 10 μg of PD1-CRISPR-Cas9 plasmids, which were intracellularly delivered to the nearby tumor draining lymph node (TdLN) tissue by using the hydro-EP (PD1-CRISPR-Ele group). All the animals were euthanized and analyzed 19 days after tumor induction (Fig. 3a). Compared to animals in different control groups, PD1-CRISPR-Ele treatment showed significantly better anti-tumor efficacy in terms of restricting tumor growth and maintaining animal survival over the experimental window (Fig. 3b–e). A diffusive local delivery of the same amount of PD1-CRISPR-Cas9 plasmids to the lymph node (no electrical trigger, denoted as PD1-CRISPR-Diff) or intramuscular injection of 100 μg (IM-DNA-injection, 10 times more DNA) PD1-CRISPR-Cas9 plasmids only showed marginal anti-tumor effects over the untreated animals. Notably, intramuscular injection of nucleic acids is very commonly used for DNA-based cancer immunotherapy practices[25–27], but this approach showed non-comparable anti-tumor efficacy as the PD1-CRISPR-Ele treatment even at a 10-fold DNA dose, suggesting that the localized in vivo T-cell gene-editing is a highly effective approach to enhance ICB-based cancer immunotherapy[28,29]. Comparing PD1-CRISPR-Ele *vs* IM-DNA-injection cases, the allowance of a substantially lower dose of DNA usage also prevents potential side effects that might cause unexpected damages in different organs[30] (Supplementary Fig. 11). If the guide RNA for PD1 were removed from the CRISPR-Cas9 plasmid (Null-plasmid-Ele), the anti-tumor therapeutic efficacy was almost completely gone, thus ruling out the effects of DNA electroporation for immunity activation. Interestingly, in a positive control group of intravenous injection of anti-PD1 antibody (anti-PD1-Injection), we observed some level of anti-tumor efficacy, but it was far less effective than the hydro-EP treatment, suggesting the great therapeutic potential of the in vivo T-cell engineering approach. We further found that the choice of lymph nodes also made a difference in the anti-tumor efficacy, the non-TdLN electroporation (nonTdLN-PD1-Ele) showed mediocre performance (Fig. 3b–e), implying a critical role of an efficient crosstalk between the engineered lymph node and the tumor site for achieve the best anti-tumor efficacy.

To study the immunity activation underlying the observed anti-tumor effects, we collected the tumor tissues from the experimental animals to examine the immune cell infiltration in response to PD1-CRISPR-Ele treatment on day 19 after tumor inoculation. By immunostaining of the tumor tissues, we found that the mice treated with PD1-CRISPR-Ele showed significantly more infiltration of $CD4^+$ and $CD8^+$ cells in comparison to the animals in the control groups, which is consistent with the results observed at the lymph node tissues (Fig. 3f–h, and Supplementary Fig. 12). Flow cytometry analysis also showed that PD1-CRISPR-Ele mice had significantly higher percentage of infiltrated $CD3^+$, $CD4^+$, and $CD8^+$ cells in the extracted tumors (Fig. 3i). The proportion of $CD8^+$ cytotoxic T lymphocytes (CTLs), which are the major players providing the antitumor immunity, increased by nearly 6-fold in the PD1-CRISPR-Ele treated mice in comparison to the untreated animals, and by nearly 3-fold over that of the IM-DNA-Injection treated mice. Similarly, the percentage of $CD3^+CD4^+$ or $CD3^+CD8^+$ in tumors extracted from PD1-CRISPR-Ele mice was remarkably increased (Supplementary Figs. 13, 14).

To verify that the tumor infiltration T-cells came from the translocation of the gene-edited PD1-deficient T-cells from nearby TdLN, the $CD4^+$ and $CD8^+$ T-cells extracted from the tumors were then examined for their expression of PD1 along with immunity related biomarkers. Not surprisingly, the $PD1^-$ portion of $CD3^+CD4^+$ T-cells was significantly increased in the tumor tissues extracted from the PD1-CRISPR-Ele mice (36.7 ± 3.7% vs. 16.8 ± 1.2%, PD1-CRISPR-Ele *vs.* untreated); similar increase was also observed for the $PD1^-$ portion of $CD3^+CD8^+$ T-cells (36.1 ± 7.2% vs. 13.7 ± 1.1%, PD1-CRISPR-Ele *vs.* untreated, Supplementary Fig. 15), supporting our reasoning of enhanced infiltration of CRISPR-Cas9-edited T-cells as a result of induced anti-tumor immune responses. To differentiate the antigen-experienced $PD1^-CD3^+$ T-cells (PD1 knockdown by hydro-EP) from the naïve $PD1^-CD3^+$ T-cells (no tumor-antigen experience) in the tumor microenvironment (TME). CD44 was used as an indicator for antigen-experienced cells[31], thus $PD1^-CD44^+$ T-cells were the immune cells infiltrated to TME after the hydro-EP treatment. Our findings revealed that in PD1-CRISPR-Ele animals, approximately 16.2% of the $CD3^+CD8^+$ T-cells were of identified as $PD1^-CD44^+$. This number is negligibly low for the untreated or null-plasmid-Ele groups (Fig. 4a, b), indicating not only a success of PD1 knockdown in antigen-experienced T-cells, but also showing their effective infiltration into TME for anti-tumor therapeutic efficacy.

Furthermore, we examined the exhaustion status of the infiltrated T-cells, which is marked by the dysfunction in proliferation and effector function[32,33]. The proliferation marker Ki67, the cytotoxic protein GrzB, and T-cell inhibitory receptor Tim-3, related to cell exhaustion and restoration were examined (Fig. 4c–e). The population of infiltrating $Ki67^+CD8^+$ and $GrzB^+CD8^+$ T-cells was increased by more than 5- and 7-fold in comparison to the untreated group (Fig. 4c, d), indicating the existence of a notable number of effector $CD8^+$ T-cells in the TME for the PD1-CRISPR-Ele group. The amount of exhausted $Tim\text{-}3^+CD8^+$ in the $CD3^+$ T-cells in TME was also

https://doi.org/10.1038/s41467-024-54292-0

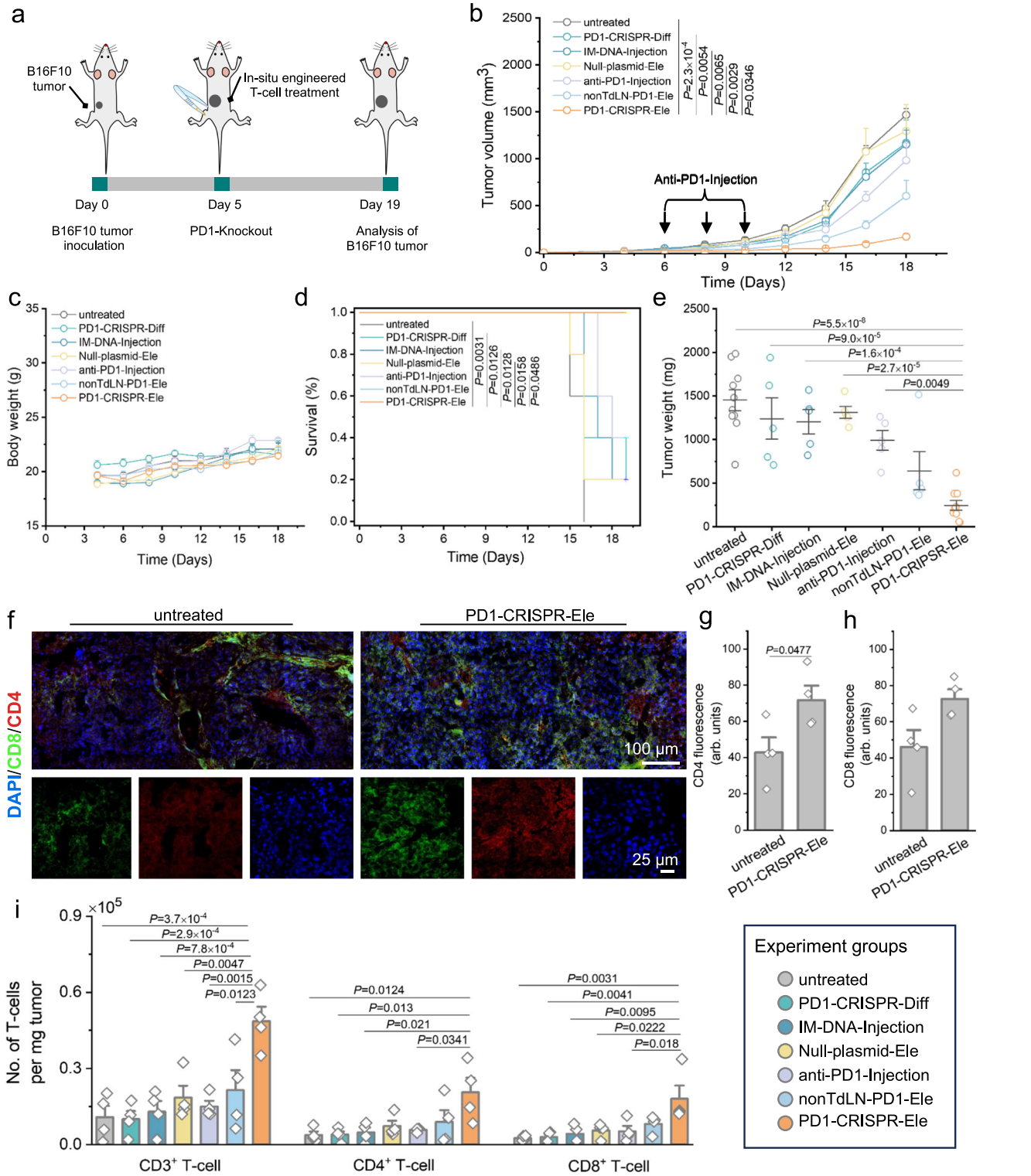

Fig. 3 | Systemic anti-tumor immune response induced by localized in vivo T-cell gene-editing. a Schematic illustration of in vivo T-cell engineering treatment in mice. Tumor volume (**b**), body weights (**c**) curves for mice received different treatments as indicated. **d** Kaplan–Meier plots of the overall survival for animals in different groups. Log-rank tests were performed to analyse the overall survival. For (**b**–**d**), $n = 5$ mice in each group. **e** Tumor weight of excised tumors at day-19, $n = 5$ or 10 mice in each group (10 for PD1-CRISPR-Ele and untreated groups, 5 for other groups). Fluorescence microscopy images (**f**) and fluorescence quantitation (**g**, **h**) of the excised tumors after different treatments. Scale bar, 100 μm. Scale bar, 25 μm in the enlarged view, $n = 4$ independent samples. **i** Evaluation of tumor-infiltration of $CD3^+$, $CD4^+$, and $CD8^+$ T-cells 19 days after various treatments as indicated, $n = 4$ mice in each group. The data are presented as mean ± s.e.m. Statistical significance was calculated by two-sided Student's t-test for two group comparison, one-way ANOVA with Tukey's test for multiple comparisons. Experimental group information: mice received no treatment (untreated), mice received PD1-CRISPR-Cas9 plasmid in TdLN without electroporation (10 μg, PD1-CRISPR-Diff), mice received intramuscular injection of PD1-CRISPR-Cas9 plasmid (100 μg, IM-DNA-Injection), mice received intravenous injection of anti-PD1 antibodies (20 μg/injection, 3 injections, anti-PD1-Injection), mice received TdLN electroporation of CRISPR/Cas9 plasmid minus gRNA (Null-plasmid-Ele), mice received non-TdLN electroporation of PD1-CRISPR-Cas9 plasmid (10 μg, nonTdLN-PD1-Ele), and mice received TdLN electroporation of PD1-CRISPR-Cas9 plasmid (10 μg, PD1-CRISPR-Ele). Source data are provided as a Source Data file.

https://doi.org/10.1038/s41467-024-54292-0

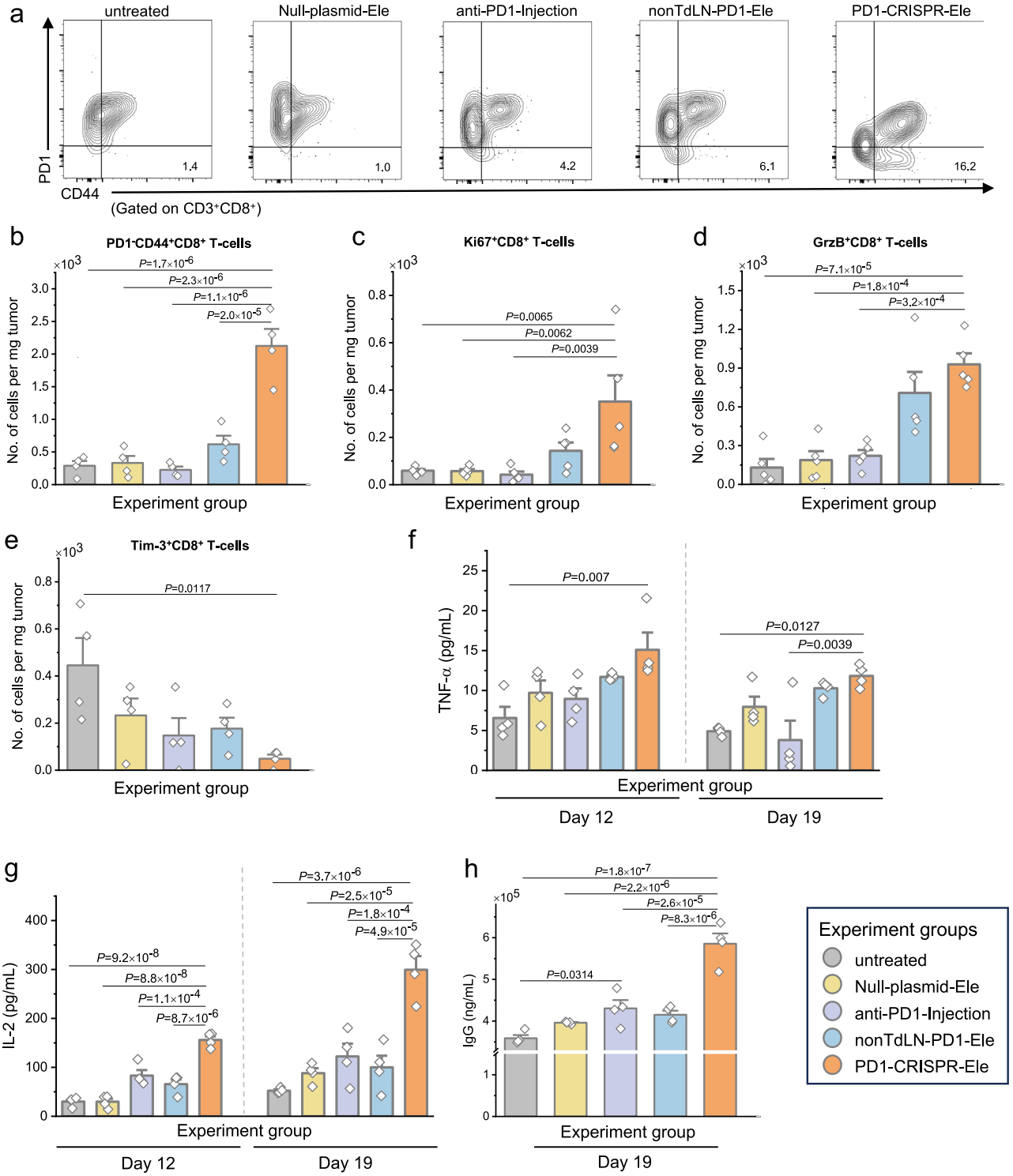

Fig. 4 | Characterization of T-cells infiltration and anti-tumor immunity in the tumor microenvironment (TME). Determination of antigen-experienced PD1⁻ T-cells in TME. Flow cytometric analysis (**a**) and quantification (**b**) of the tumor-infiltrated PD1⁻CD44⁺CD8⁺ T-cells 19 days after different treatments, $n = 4$ mice in each group. (**c**–**e**) Analysis of the activation and exhaustion status of the infiltrated T-cells. Quantification of tumor-infiltrated Ki67⁺CD8⁺ (**c**), GrzB⁺CD8⁺ (**d**), and Tim-3⁺CD8⁺ (**e**) T-cells 19 days after the indicated treatments. For (**c**, **d**), n = 5 mice in each group. For (**e**), $n = 4$ mice in each group. **f**–**h** Evaluation of cytokines levels as the result of anti-tumor immune response. Concentrations of different cytokines: TNF-α (**f**), IL-2 (**g**), and IgG (**h**) in the serum of mice received different treatments. For (**f**–**h**), $n = 4$ mice in each group. The data are presented as mean ± s.e.m., analyzed using a one-way ANOVA with Tukey's multiple comparison test. Source data are provided as a Source Data file.

significantly decreased (Fig. 4e), further providing the evidence for the infiltration tumor-specific CD8 T-cells in the hydro-EP treated animals and an effective engagement of the ICB therapeutic strategy. Additionally, the serum level of different cytokines, TNF-α, IL-2, and immunoglobulin G (IgG) in PD1-CRISPR-Ele treated mice were significantly increased at different assessment time-points (Day 12 and Day 19), when compared to the control groups (Fig. 4f–h), proving that the targeting of TdLN plays a crucial for achieving the anti-tumor

https://doi.org/10.1038/s41467-024-54292-0

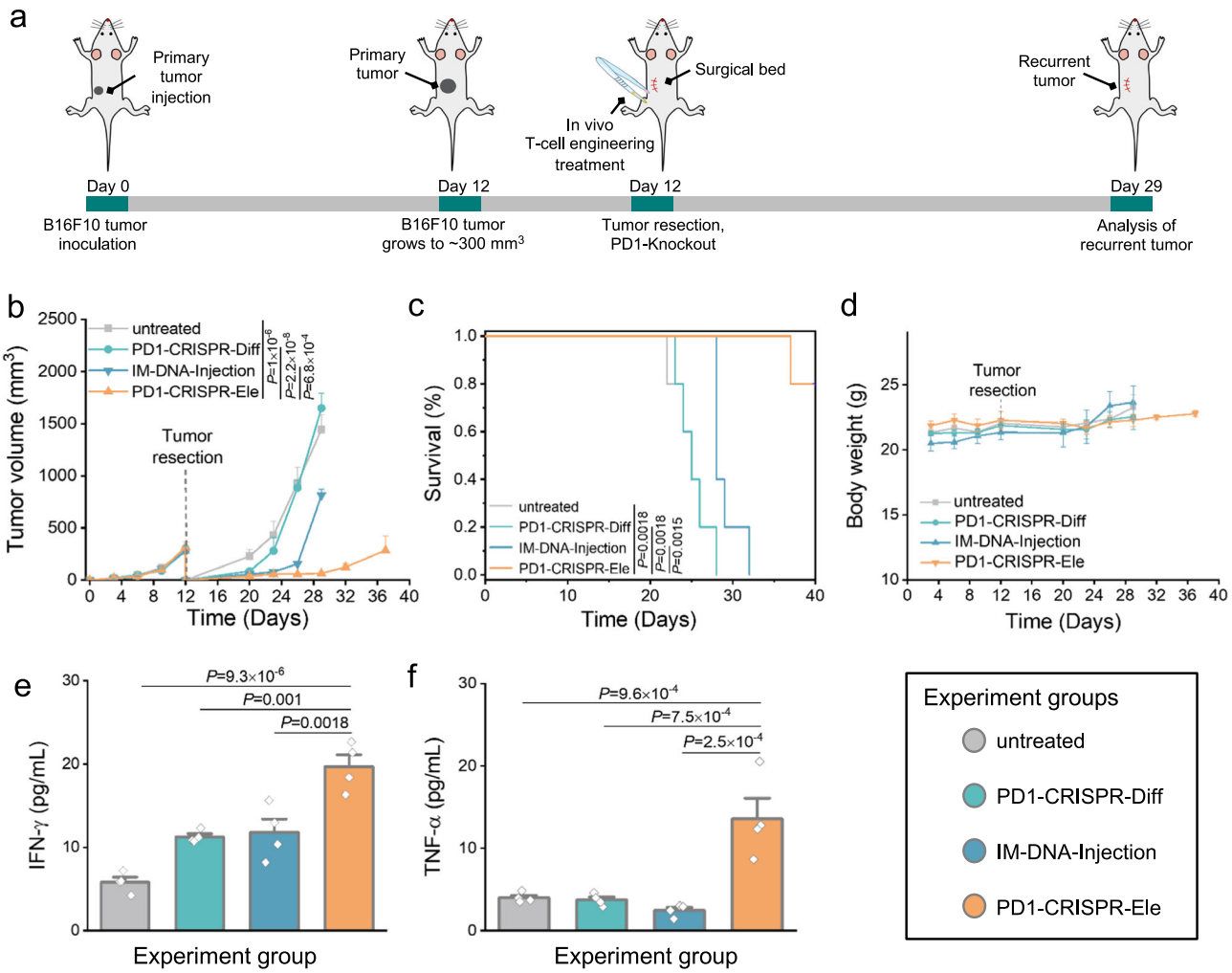

Fig. 5 | Localized in vivo gene-editing reduces recurrence of B16F10 melanoma tumors in the surgical bed. (**a**) Schematic illustration of in vivo T-cell engineering treatment in an incomplete-surgery murine tumor model. The tumor growth (size) (**b**), survival curves (**c**), and body weights (**d**) after different treatments as indicated. For (**b**–**d**), $n = 5$ mice in each group. Log-rank tests were performed to analyse the overall survival. Cytokine concentrations of IFN-γ (**e**) and TNF-α (**f**) in the serum of mice on day 19 with different treatments. For (**e**, **f**), $n = 4$ mice in each group. The data are presented as mean ± s.e.m., analyzed using a one-way ANOVA with Tukey's multiple comparison test. Source data are provided as a Source Data file.

efficacy by promoting both cell-mediated adaptive immunity and humoral immunity.

Prevention of tumor recurrence at postsurgical stage

To test the capability of the localized in vivo gene-editing in lymph node as a therapeutic approach to in the post-surgical stage for preventing tumor recurrence, we next performed an experiment using a B16F10-based tumor recurrence model[34]. After surgically removing the majority of the tumor tissues in B16F10-injected mice, the animals received PD1-CRISPR-Ele treatment in the nearby lymph nodes, which were likely to become the tumor draining ones (TdLN) if anti-cancer immunity is induced (Fig. 5a). Over the experimental period, the tumor growth burden was monitored and quantified by using caliper measurements every 2 or 3 days. Remarkably, we found that the PD1-CRISPR-Ele mice exhibited only minor tumor relapse, and 80% of the animals showed no detectable tumor recurrence. In contrast, the control mice treated with IM-DNA-injection of the same DNA at a 10-fold dose (100 μg) only showed a slight delay but still significant recurrent tumor growth; almost no preventive anti-tumor-recurrence effect was observed if the CRISPR DNA was locally delivered to lymph nodes by diffusion without electroporation (PD1-CRISPR-Diff) (Fig. 5b, Supplementary Fig. 16). 80% of the PD1-CRISPR-Ele mice survived after the whole 40-day experiment period without significant loss of body weight, while none of the animals in different control groups survived beyond day 35 (Fig. 5c, d). In consistent with the anti-tumor-recurrence efficacy, the level of cytokines secretion, including IFN-γ and TNF-α were both significantly elevated (Fig. 5e, f), which provided substantiated effective humoral immune response induced by PD1-CRISPR-Ele treatment.

Restriction of metastatic secondary tumor growth

Furthermore, the in vivo T-cell engineering enhanced ICB was tested in a more clinically relevant ectopic tumor recurrence model (Fig. 6a), which mocks a more malignant tumor recurrent growth. In this experiment, one C57BL/6 mouse was subcutaneously injected with B16F10 melanoma cells on one side of its flank to induce a first primary tumor, which was surgically removed later; and a secondary tumor was inducted on the other side of the mouse flank to form an ectopic tumor recurrence model to mimic cancer metastasis[35]. In conjugation with the second tumor cell injection, PD1-CRISPR-Ele was performed in a lymph node for in vivo T-cell engineering. As shown in Fig. 6, mice receiving PD1-CRISPR-Ele treatment were protected from tumor recurrence with the smallest tumor relapse and significantly higher survival rate when compared with the animals in different control groups (Fig. 6b–e). It is noted that mice receiving PD1-CRISPR-Ele treatment exhibited superior prognosis effect.

https://doi.org/10.1038/s41467-024-54292-0

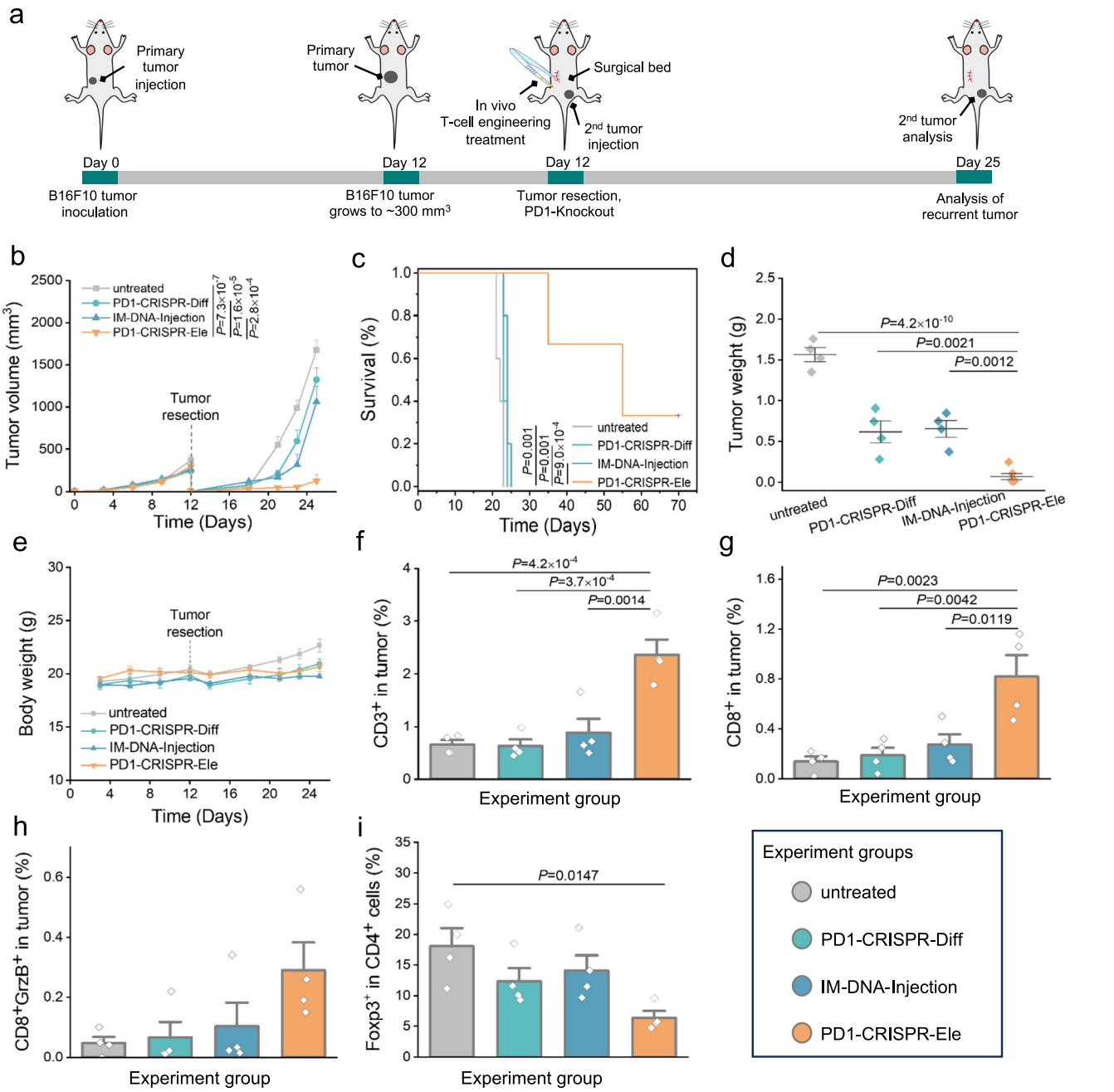

Fig. 6 | Localized in vivo gene-editing inhibits the postsurgical recurrence effectively. (**a**) Schematic illustration of in vivo T-cell engineering treatment in a murine ectopic tumor recurrence model. The tumor growth (size) (**b**), survival curves (**c**), tumor weights (**d**) and body weights (**e**) are presented. For (**b**, **c**, **e**), 5 and 6 mice were analyzed (6 for PD1-CRISPR-Ele group, 5 for other groups). For (**d**), 4 and 6 mice were analyzed (6 for PD1-CRISPR-Ele group, 4 for other groups). Log-rank tests were performed to analyse the overall survival. Quantification of the proportion of $CD3^+$ (**f**) and $CD8^+$ (**g**) T-cells in the extracted tumor upon various treatments. **h** The percentage of the tumor-infiltrated $CD8^+GrzB^+$ T-cells in the tumor. **i** The percentage of $Foxp3^+$ cells in $CD4^+$ T-cells in tumor tissues collected from the treated mice. For (**f**–**i**), $n = 4$ mice in each group. The data are presented as mean ± s.e.m., analyzed using a one-way ANOVA with Tukey's multiple comparison test. Source data are provided as a Source Data file.

Animals in this group showed multi-fold longer survival span and 1/3 of the mice were sacrificed after more than 70 days with a nearly complete alleviation of cancer-related symptoms (Fig. 6c). A remarkable increase of the $CD8^+$, $CD3^+$ and $CD4^+$ cells was observed in the extracted tumor tissue in PD1-CRISPR-Ele mice (Fig. 6f, g, and Supplementary Figs. 18–21). The proportion of cell $CD8^+$ co-expressing GrzB was also significantly increased (Fig. 6h). In addition to higher and more efficient infiltration of CTLs in the tumor tissue, the percentage of regulatory T-cells (Treg, $CD3^+CD4^+Foxp3^+$) was substantially decreased in the experimental mice (Fig. 6i). Collectively, these results suggest that localized gene-editing in lymph node is an effective approach to produce engineered PD1-deficient T-cell in vivo to improve ICB-based cancer therapy.

Discussion

In this study, we develop an in vivo gene edit strategy for improving ICB cancer therapy. The approach uses the hydro-EP to enable nucleofection of PD1-targeted CRISPR-Cas9 DNAs into T lymphocytes directly within lymph node tissues, and subsequently produces engineered T-cells with suppressed PD1 to combat tumor growth,

metastasis and recurrence. We showed that the hydro-EP system could efficiently deliver CRISPR-Cas9 DNAs (guided to delete PD1) into T-cells within lymph nodes to produce PD1-deficient T-cells in living animals in a minimally invasive manner. Our results show that a single localized in vivo electroporation by hydro-EP was sufficient to achieve successful gene editing in the T lymphocytes locally in the lymph node without significantly affecting other types of cells; and the engineered T lymphocytes can reliably and efficiently infiltrate into the targeted B16F10 tumor at a result of enhancement of systemic antitumor immunity in tumor-bearing mice.

From a technical perspective, we provide a feasible and efficient approach to produce engineered T-cells in vivo by localized gene-editing. For therapeutic purpose, current gene delivery technologies, such as viral-based methods, lipid-material facilitated lipofection, and many nanoparticle-assisted systems are usually accompanied by stochastic gene delivery, laborious fabrication and unexpected side effects (e.g., inflammatory response and cell death), etc.[36,37]. With our approach, simply by a brief and direct contact with lymph node tissue, micro/nano charged molecules in the hydrogel electrodes can be induced to release under an applied electrical field to enable the controlled release of the preloaded therapeutic agents (DNA, RNA, chemical agents, etc.) to the targeted tissues[38,39]. Particularly in this study, after the PD1-CRISPR-Cas9 DNAs were expelled from the hydrogel matrix to intercellular mesenchymal space of the lymph node, a highly focused electric field was applied to perform in vivo electroporation to allow cytosolic delivery, in-situ gene transfection and then gene editing to inhibit PD1 expression in T-cells[23,37]. The two-phase operation for in vivo gene delivery, including release of nucleic acids and cellular electroporation, was conducted consecutively by using a single-component hydrogel device to deliver naked DNAs into lymph node T-cells in a highly convenient, and footprint-free manner, which eliminates the risk of uncertain allergic side effects caused by viral or lipid nanoparticle facilitated in vivo gene transduction[40,41]. Conventionally, bulk tissue electroporation typically uses fixed sharp needle electrodes, which can potentially cause discomfort, scarring, and risk of infection after a treatment[25,36,37]. The pre-shaped hydrogel hWE used in this study has a low Youngs' Modulus (0.73 ± 0.16 Mpa) similar to soft human tissues and is much less irritative[42]. It is noted that the hydrogel hWE was made into a microneedle structure, which assists the NA delivery in a minimally invasive manner, and decreases prognosis damage of lymph node[43]. The dosage of delivered nucleic acid can also be delicately controlled by the pre-loading of NAs and by adjusting the applied electric field for in situ electrophoresis[44,45]. As a low-cost disposable device, the hWE is made of (Polyvinyl alcohol) PVA and PEDOT:PSS, which are all widely used medical materials with little biocompatibility issues. Particularly, PVA has been used in FDA-approved drug products, emphasizing the great promise for clinical translation of the hWE system. As demonstrated in this study, a hydrogel-based in vivo electroporation system was employed to enable efficient in situ gene editing in a targeted, safe and feasible way.

It is known that electroporation-mediated intracellular delivery is not specifically oriented towards any cell species. While our ideal targets are the T-cells in a lymph node, off-target transfection in other cell types is also possible. Generally, lymph nodes are regarded as highly specialized microenvironments for mounting effective immune responses, the majority of the cell population are immune cells (T-cells, approximately 65–78%; B-cells, around 9–15%), with addition of a small percentage of stromal cells, dendritic cells, macrophages, and others[46]. Therefore, it is expected to see that the majority of hydro-EP transfected cells are immune cells. In our experiments with eGFP transfection in a lymph node, the transfected cells contained ~75.6% of $CD3^+$ T-cells, 15.1% $CD19^+$ B cells, 4.2% $CD11c^+$ dendritic cells, and 1.5% $NK1.1^+$ natural killer cells, and a small portion of other cell types (3.6%) (Fig. 2). We believe that the dominant genetic engineering in the targeted T-cells provides a first level insurance to limit the side effects associated with "off-target" knockdown. Furthermore, the use of CRISPR-Cas9 based gene-editing tool and proper guide sequence ensure a second-level control to only affect T-cells expressing PD1, which are immune cells that have prior experience of tumor antigens[47]. PD1 negative cells remain unaffected even if they receive exogenous delivery of DNAs. It is noted that, apart from T-cells, PD1 could also be expressed on NK cells, B cells, and some myeloid cells[48], there are studies showing that PD1 blockade in B cells enhances their proliferation and cytokine production[49]. Our data also suggests that the existence of transfected B-cells does not compromise the immune response at the cytokine (e.g., TNF-α, IL-2, and IgG) secretion level (Figs. 3, 4); DNA transfection of a small portion of non-T-cells did not show any adverse effects that compromise the anti-tumor efficacy in our study. In the future, the creation of vector systems with cell-specific promoters could further enhance the specificity of the in vivo gene editing by using the hydro-EP system to improve the safety of the associated therapies.

From a therapeutic perspective, in most of the current clinical practices involving engineered T-cells, ex vivo cell manipulation remains a prerequisite. The procedure typically includes peripheral blood mononuclear cell collection, in vitro T-cell transduction via viral or electroporation approaches, T-cell expansion and a final infusion of engineered T-cells back to patients[12,15]. The in vivo T-cell engineering approach bypasses many uncertainties from in vitro cell engineering, and dramatically simplifies the whole therapeutic process. First, it eliminates the discomfortable experience of cell collection from patients[50,51]. Secondly, the hWE device can be made as a consumable one-time-use supply to enable equipment-independent in vivo T-cell engineering, which would otherwise be limited by cell culture facilities and critical transportation conditions for in vitro practices[16,50,52,53]. Thirdly, our method adopts a minimal invasive operation to electroporate T-cell to achieve high nucleofection efficiency and the whole operational process could be completed in ~20 mins. The brief treatment time not only improves patient compliance but also make it more suitable for repeated treatment if mRNAs are to be introduced for transient gene editing. While, in this study, we provided a proof-of-concept demonstration of in vivo gene-editing of T-cells in a rodent model, the specific operational parameters, such as therapeutic contents, electroporation time, frequency, dosage, etc., can be readily adjusted for other model subjects for optimized therapeutic efficacy. For example, higher PD1-CRISPR-Cas9 plasmid dose or larger device dimension might induce more potent therapeutic outcomes in larger animal models. Such expandability further enables an easy clinical translation of the hydro-EP technique as a safe and feasible in vivo T-cell engineering based cancer therapy in the future.

Particularly, different demonstrations were performed for mimicking various clinical scenarios could potentially use hydro-EP for enhanced ICB therapeutic outcomes. For experiments outlined in Fig. 3, PD1 knockdown was performed after the establishment of B16F10 tumors, accordingly the expected therapeutic efficacy is the restriction or elimination of primary tumor growth. For experiments outlined in Fig. 5, PD1 knockdown on the lymph node was performed after the surgical removal of the primary tumor, therefore the expected therapeutic outcome would be a prevention of tumor recurrence at the postsurgical stage. For experiments documented in Fig. 6, PD1 knockdown was tested in a more clinically relevant ectopic tumor recurrence model, where secondary tumor already occurred after the surgical removal of the primary tumor (recurrence), the expected therapeutic outcome is a restriction or elimination of the metastatic secondary tumor. The targeted clinical scenarios are indeed represented by cancer progresses of different stages, which may have different responses to anti-cancer treatments, including the ICB therapies, in human patients[35].

As a promising alternative for improving cancer immunotherapy, our approach showed significantly better anti-tumor efficacy over the

control group involving intravenous injection of anti-PD1 antibodies, which is usually adopted in the current ICB therapies. The required long-term drug administration is likely to cause limited objective responses, low drug utilization and frequent toxicity. The antibodies, like avelumab, durvalumab, or combinations of nivolumab and ipilimumab, etc., are also cost prohibitive[3,4]. Beyond the efficacy concerns, critical storage and transportation conditions are usually required over a comparatively long treatment period, which is not friendly to the patient in less developed regions[54,55]. In contrast, the in vivo T-cell engineering therapy creates PD1-deficient T-cells and provides longer blockage of immune checkpoints by eliminating PD1 gene loci of T-cell with a one-shot minimal-invasive operation. The engineered T-cells could proliferate in vivo to work as an "everlasting drug" to restrict tumor growth and prevent cancer relapse. In the B16F10 melanoma model used in this study, the treated mice generate a systemic anticancer immune response with an effective production of PD1-deficient T-cells, as evidenced by a multi-fold increase of infiltrated $CD4^+$ and $CD8^+$ T-cells in the TME, without getting exhausted (Fig. 4). The translational potential is further supported by a recent phase I clinical trial showing that the patients experienced successful engraftment of PD-1-deficient T-cells do not develop any autoimmune problems[12].

It was interesting to find that the choice of lymph node for PD1 knockdown has a profound impact on the anti-tumor therapeutic efficacy, which echoes some emerging data showing TdLN-targeted treatments for enhancing the efficacy of ICB therapy[56,57]. Upon tumor occurrence, antigen-presenting cells (APCs) are transported to tumor-draining lymph nodes (TdLNs), where they stimulate prime naïve T-cells, transforming TdLNs into dynamic a reservoir of increasingly activated T-cells[3]. The activation process is crucial for the engagement of TdLNs in our improved ICB antitumor therapy. As the T-cells start to express PD1 after tumor-antigen activation, the percentage of $PD1^+CD8^+$ T-cells is therefore higher in the TdLNs (compared to other non-TdLNs), underscoring higher efficiency of PD1 knockdown and subsequent creation of tumor-combating effector T-cells from the TdLN. The CRISPR-Cas9 plasmid was chosen for targeted editing of PD1 gene, which was proved by recent clinical studies to have low chances of off-target editing, especially when relevant gene delivery is achieved by physical approaches like electroporation, when compared to the use of virus-based delivery methods[12,15]. The footprint-free in vivo intracellular delivery, achieved by using our conductive hydrogel-based electroporation system, offers better safety control for in vivo gene editing practices. For clinical translation of the hydro-EP technique, the scale of human tissues differs from the demonstrated rodent animals, therefore the geometric and structural parameters of the hWE electrode likely need further optimization. Adjustments in the therapeutics loading, and electroporation parameters may also be explored. The clinical practice of lymph node biopsy can be seamlessly integrated with the hydro-EP technique, where the hydro-EP forcep is applied to one or multiple tumor-draining lymph nodes (TdLNs) within the tumor-draining basin, only requiring minimally invasive surgery due to the localized distribution.

While we used PD1-CRISPR-Cas9 DNA as a demonstration here, the in vivo T-cell engineering approach is readily compatible with other types of therapeutics. For example, cancer-specific TCR transgenes can be used to specifically detect and kill tumor cells, providing a path for chimeric antigen receptor (CAR) T-cell therapy[58]. Moreover, transient genetic editing tools can also be considered to use with the conductive hydrogel-based electroporation system. Especially, mRNAs encoding the Cas9/Cas13 protein are likely to improve the gene editing efficiency and to further reduce the risks of chromosome insertion and off-targeting edit[59–61]. Multiplexed genome editing is also possible to be implemented in vivo by building "all-in-one" CRISPR/Cas systems containing several gRNA expression cassettes[62]. Finally, this approach is not limited to lymph node tissues, it is certainly possible that the in vivo gene editing method can be customized to perform cell engineering in other organ systems. For example, fibroblasts can be induced to differentiate into cardiomyocyte-like cells for cardiac regeneration[63]; wound-resident mesenchymal cells can be transduced and reprogrammed towards expandable epithelial tissues[64]. Such a platform technique for in vivo cell engineering provides a promise for a scalable and affordable gene-editing alternative to address many diseases.

Methods

Ethical regulations

The research presented here complies with all relevant ethical regulations. All experiments involving animals were conducted following protocols approved by the Animal Ethical Committee of City University of Hong Kong (CityU) and Department of Health of Government of HKSAR ((20-232) in DH/HT&A/8/2/5/Pt.7). The maximal tumor burden permitted by the Animal Ethical Committee of City University of Hong Kong was the weight of tumor should not exceed 10% of body weight. In any of animal experiments described in this article, the maximal tumor size of the mouse was never reached.

Cell lines and materials

PVA were purchased from Sigma-Aldrich with the molecular weights at 89,000–98,000. The mouse melanoma cell line, B16F10 and HEK293T cells were purchased from the American Type Culture Collection. All other reagents and solvents were purchased from Sigma-Aldrich. The reagents used for cell and animal related experiments are mostly from Thermo Fisher Scientific. The materials from other vendors are specified accordingly otherwise.

Construction of PD1-CRISPR-Cas9 plasmid

To construct *PDCD1* targeting plasmids, plasmid PX330 was digested with Bbsl and sgRNA targeting *PDCD1* (5′-CACCGTGCCTCGGCCATGGGACGT-3′) was annealed so that the sticky ends sequence match Bbsl ends of PX330. After ligation, the cloned plasmids were confirmed by DNA sequencing. pX330-U6-Chimeric_BB-CBh-hSpCas9 (PX330) was purchased from Addgene (Plasmid #42230).

Animals

Female C57BL/6 mice (6–8 weeks) were acquired from Laboratory Animal Research Unit (LARU) of CityU, and were maintained following standard guidelines. The sample size were determined using power analysis with a target power of 0.8 (80%). This value was chosen to ensure a high likelihood of detecting a true effect while minimizing the risk of false negatives. The parameters for the power analysis, including expected averages and standard deviations. Depending on specific experiments, a group size of 4 to 6 animals per condition would typically be sufficient. This range was chosen to balance statistical power with ethical considerations, ensuring that we used the minimum number of animals necessary to achieve reliable results. The sample size for each experimental group is explicitly stated in the figure captions and data descriptions. No data was excluded from the analyses.

Fabrication of hydro-EP device

The hydrogel-based electroporation device (hydro-EP) consists of two electrodes assembly integrated on the edge of the surgical forceps, including a hydrogel-based working electrode (hWE) and metal-based ground electrode (mGE). To be specific, hWE were prepared using PDMS molds with the array of pyramid holes (base diameter of 400 μm, height of 1000 μm). The prepared hydrogel precursor solution (15 wt% PVA and 0.3 wt% PEDOT:PSS mixture) with the specific plasmid content (10 μg) was directly deposited by pipetting onto the PDMS mold surface, which was pretreated with plasma. After desiccation was completed in room temperature, the formed hWE were carefully sperateted from the PDMS molds. mGE is a layer thin metal

substrate, about 200 μm thick, 2 × 2 mm^2 square. Both mGE and hWE were fixed at the tip of surgical forceps on the electrical interconnects, linked with an external voltage supplier (Supplementary Fig. 1). The authors affirm that human research participants provided informed consent for publication of the images in Fig. 1b, c and Supplementary Fig. 1a.

Mechanical strength test

The mechanical tensile stress–strain evaluation was carried out by the uniaxial tensile test employing an Instron materials test system (Instron 5942 Mechanical Tester) equipped with a 500 N tension sensor at room temperature. PVA&PEDOT:PSS composite hydrogel was immersed into 1× PBS solution until equilibrated swelling state. After the removal of superfluous water on the surface, the hydrogel sample was prepared in standard shape (65 mm in length × 14 mm in width × 0.2 mm in thickness). The Young's modulus was calculated from the slope of the stress-strain curve, where the test speed was 2 mm/min (Supplementary Fig. 2).

The mechanical strength of hWE was evaluated by pressing vertically with Instron materials test system (Instron 5942 Mechanical Tester). Briefly, the test station sensor was set to vertical move at the speed of 0.1 mm/min. The displacement and force curves were recorded when the upper stainless force sensor began to touch with hWE tips until when the hWE began to buckle (Supplementary Fig. 2).

Surgical procedures and in vivo T-cell engineering

Before the in vivo T-cell engineering procedure, a B16F10 solid tumor model was established firstly. 1×10^6 B16F10 cells was subcutaneous injected into the flank of C57BL/6 mice. After 5 days, the tumor formed in a small black lump. For surgery, 6–8 week-old mice were anaesthetized with pentobarbital sodium (40 mg/kg, i.p., Ceva Santé Animale). Another I.P. injection of atropine (3.25 mg/kg) was performed to suppress bronchial secretion that may cause suffocation. The flank were carefully shaved and an ~0.5 cm incision above on the inguinal lymph node was made, and the lymph node located, which was applied with hydro-EP for localized in vivo electroporation. The targeted lymph node was carefully sandwiched by the forceps-type of hydrogel device. During the electroporation process, a source meter (Keithley 2612B System) was employed to connect with our hydrogel platform to supply 1 V d.c. voltage to trigger preloaded molecular release from hydrogel matrix for 20 min. Afterward, a waveform generator (Keysight 33500B series) and electrical stimulator (A.M.P.I.) were connected with our hydrogel platform to supply 90 V pulse waves with a width of 50 ms, and 10 pluses to introduce transient pores on the plasma cell membrane. These pules facilitating efficient DNA cargos transfer to cells in vivo. After the in vivo electroporation procedure, the lymph node site was rinsed with 1× PBS solution to avoid unnecessary tissue adhesion. The wound was sutured by the Autoclip wound clip system with 9-mm nails. Throughout the all experiment procudures, a heating pad was placed beneath the animal to maintain a stable temperature at 37 °C (Supplementary Fig. 8).

Lymph nodes analysis

On day 7 after the in vivo T-cell engineering treatment, the inguinal lymph nodes were surgically removed from the experimental mice. The harvested lymph nodes were ground with the end of a sterile syringe to get a homogenized lymphocytes solution by treated with a 70 μm cell strainer. The cell suspension collected from engineered lymph nodes was then stained with anti-mouse PD1, anti-mouse CD3, anti-mouse CD4, anti-mouse CD8α, anti-mouse CD137, anti-mouse NK1.1, anti-mouse CD19, and anti-mouse CD11c to analyze the different lymphocyte subsets with PD1 expression by flow cytometry (BD Biosciences, BD FACSDiva software v 8.0).

Creation of 3D cell culture for a tissue mimicry

Gelatin methacryloyl (GelMA)-based hydrogel was used for 3D culture of HEK293T-cells to create an ex vivo model for optimizing the hydro-EP parameters[65]. Lyophilized GelMA (7.5 *wt%*) was dissolved in PBS with addition of the photoinitiator (0.5 *wt%*, 2-hydroxy-1-(4-(hydroxyethoxy) phenyl)−2-methyl-1-propanone, Irgacure 2959, CIBA chemical) at 80 °C. The cells were suspended in the GelMA prepolymer solution at a concentration of 4×10^6 cells/mL. The cell-prepolymer mixture was crosslinked upon a UV (365 nm) light irradiation to form a 3D tissue mimicry. Approximately 200,000 cells were densely packed in a piece of GelMA hydrogel (2 mm in height, 6 mm in diameter). The cell-laden was cultured in DMEM containing 10% fetal bovine serum (FBS) and 1% penicillin streptomycin (PS).

Optimization of hydro-EP parameters

For ex vivo optimization of hydro-EP electroporation parameters, the hydro-EP device was applied to the cell-loaded GelMA hydrogel to mimic the device-tissue interface of the in vivo electroporation of a lymph node. Intracellular delivery and cellular transfection of eGFP DNAs were performed for quantification purpose (Supplementary Fig. 7). A sustained low-voltage trigger (1 V, 20 min) followed by high-voltage pulsing were applied to electroporate the cells in the GelMA matrix. Different electroporation parameters, including voltage amplitudes, pulse widths, frequencies, and number of pulses were all tested. 24 h after the electroporation, the GelMA hydrogels were enzymatically digested, the cell viability and eGFP expression were evaluated by flow cytometry and fluorescence microscopy.

Artificial activation of T-cells ex vivo

To examine the PD1 expression and knockdown in the lymph nodes, we conducted ex vivo activation of lymphocytes extracted from the lymph nodes being treated by a hydro-EP electroporation. Single-cell suspension was prepared from the treated lymph nodes extracted from a normal mouse (no tumor inoculation) 24 h after an in vivo electroporation procedure. T-cells were then isolated with a $CD3^+$ T-cell isolation kit (Biolegend). The purified T-cells (1×10^6) were then seeded in a 24-well plate, CD3/CD28 T-cell activator (DynabeadsTM, ThermoFisher) was added to the culture medium for an artificial activation. The cells were cultured in advanced RPMI 1640 Medium containing 2 mM L-Glutamine,10% FBS, 1% PS and 30 U/mL IL-2. After 48 h, the activated T-cells were harvested for analysis using flow cytometry.

Therapeutic experiment

C57BL/6 mice were weighed and randomly divided into seven groups. Specifically, mice that did not achieve any additional treatments except for tumor implantation were regarded as the negative control group to track tumor development in real-time (untreated group). The same 10 μg of PD1-CRISPR-Cas9 plasmid-loaded hWE without any external electrical stimulation (denoted as PD1-CRISPR-Diff) was chosen as a control group to simulate free diffusion. In addition, 100 μg of PD1-CRISPR-Cas9 plasmid (tenfold dose DNA agents than PD1-CRISPR-Ele group loaded) were injected intramuscularly to tumor-bearing mice serving as another control group to mimic conventional clinical choice (named IM-DNA-Injection). The tumor-bearing mice received three intravenous injections of anti-PD1 antibody (20 μg/injection, clone RMP1-14, Bio X Cell) at day 6, day 8 and day 10 after tumor inoculation serving as the clinically-relevant positive control (anti-PD1-Injection group). The tumor draining lymph node (TdLN) on mice was electroplated with CRISPR/Cas9 without gRNA sequence denoted as Null-plasmid-Ele group. The tumor-bering mice were under electroporated with PD1-CRISPR-Cas9 plasmid on non-TdLN and TdLN are denoted as nonTdLN-PD1-Ele group and PD1-CRISPR-Ele group, respectively. Both nonTdLN-PD1-Ele and Null-plasmid-Ele conduct the same surgical procedure with PD1-CRISPR-Ele, except for engineered

lymph node location or preloaded plasmid. Before 5 days of the in vivo T-cell engineering treatment, 1×10^6 B16F10 cells were subcutaneously injected into each group of C57BL/6 mice flank to make sure moderate T-cell activation. Next, the prepared device (10 μg of PD1-CRISPR-Cas9 plasmid loaded) was applied on the TdLN of mice to conduct in vivo T-cell engineering treatment. Later, the tumor sizes and mouse weights were monitored every two or three days. The tumor volumes were calculated as the following formula:

$$\text{Tumor volume} = \frac{\text{short diameter}^2 \times \text{long diameter}}{2} (\text{mm}^3) \quad (1)$$

In addition, the animal was euthanized when its tumor exceeded 2000 mm^3.

Tumor recurrence model

To further evaluate the antitumor tumor effect of in vivo T-cell engineering treatment, 1×10^6 B16F10 cells were subcutaneously transplanted into the flank of C57BL/6 mice. The tumors were surgically resected when the tumor volume reached 300 mm^3. Specifically, these tumors were resected, remaining about ~1% of tumor tissue to mimic the microtumors remaining in the surgical beds in the clinical cases. Next, the mice were randomly divided into four groups for the subsequent treatments, including the untreated group, PD1-CRISPR-Diff, IM-DNA-injection, and PD1-CRISPR-Ele. The surgical procedure of localized in vivo electroporation has been detailed and clarified hereinbefore.

A metastasis tumor mouse model was also conducted to further evaluate the treatment efficacy. 1×10^6 B16F10 cells were injected into the right flank of mice 12 days prior. On day 12, all the tumors were surgically resected clearly from mice. The mice were then selected randomly and employed for different treatment therapies. Four kinds of treatment methods were applied to these mice, including the untreated group, PD1-CRISPR-Diff, IM-DNA-injection, and PD1-CRISPR-Ele. Afterward, mice were rechallenged with 1×10^6 B16F10 on the other flank of mice to mimic the tumor transfer in the clinical cases. Briefly, during the whole surgical period, mice were anaesthetized with pentobarbital sodium, maintaining the same surgical procedures with prior part. Surgical instruments and consumers were sterile to avoid unnecessary infection. The wound was sutured by the Antoclip wound clip system (9-mm nails). The tumor size and mice weight were monitored every two or three days with a digital caliper and electronic scales, respectively.

Histological analysis

Lymph nodes, tumor tissues and main organs samples were collected for histological analysis before mice were executed. Briefly, biological tissues (lymph nodes, tumor tissues, heart, liver, spleen, lungs and kidney samples) were fixed in a PBS solution with 4 *wt%* formaldehyde for 72 h. Next, these fixed tissues were transferred into a sucrose solution (30 *wt%*) overnight, then transferred to a Cryo-OCT compound to get a frozen sample under −80 °C. The frozen samples were sectioned into 40 μm tissue slice with a Cryostar NX70 cryosectioning system. The well-preserved tissue slice can be stained for immunostaining image or H&E staining.

For immunostaining, the lymph node tissues, or cancer tissues slices were washed with 1× PBS and then permeabilized by 0.1% Triton-X 100 in PBS. Next, the washed samples were incubated in blocking solution for 2 h. The samples were then stained with 1:1000 primary antibodies (anti- mouse CD4, anti-mouse CD8a, anti-mouse CD279 (PD-1)) in a blocking solution under 4 °C overnight. The samples were washed with 1× PBS and stained with secondary antibodies for 2 fours, these slices were analyzed using a confocal microscope (Leica SP8LIA + +). For Haematoxylin-Eosin staining, the main organs slices were stained according to the manufacturer's protocol (Abcam).

Analysis of the relative abundances of T-cell populations in tumor tissues

Melanoma tumors were surgically resected and collected. Tumor tissues in different treatment strategies were cut into small pieces in a cold tumor dissociation mixture buffer, containing 1 mg/mL collagenase IV (Sigma), 1 mg/mL hyaluronidase (Sigma), and 0.2 mg/mL DNase I (Thermo Scientific). Next, the tissue mixture solution was incubated in 37 °C, 45 min to digest cancer tissue into tumor cells, following the cell filtered through a 70 μm cell strainer. The obtained tumor cell suspensions were stained with anti-mouse CD3, anti-mouse CD4, anti-mouse CD8, anti-mouse CD279 (PD-1), anti-mouse FOXP3 and anti-mouse GrzB, anti-mouse CD44, anti-mouse Ki67, and anti-mouse Tim-3 antibodies (Biolegend/invitrogen) analyzed by flow cytometry.

Cytokine detection

The serums of all mice groups were collected on day 7 or 14 after treatments and analyzed the level of immune-related cytokines. The cytokine IFN-γ, TNF-α, IL-2 and immunoglobulin G (IgG) levels were evaluated by ELISA kit (Biolegend, Thermo Scientific) according to the manufacturer's instructions.

Statistical analysis

All the experimental data in this study were subjected to statistical analysis and were expressed as mean ± S.E.M. Statistical significance ($^*P < 0.05$, $^{**}P < 0.01$, $^{***}P < 0.001$) were determined using Student's t-test for analyzing two groups. For multiple comparisons, one-way ANOVAs with Turkey's test was used. The statistical significance in overall survival was determined with a log-rank test.

Reporting summary

Further information on research design is available in the Nature Portfolio Reporting Summary linked to this article.

Data availability

The data that support the findings of this study are available within the paper, Supplementary Information, and Source Data File. Source data are provided with this paper.

References

1. Wang, C. et al. In situ activation of platelets with checkpoint inhibitors for post-surgical cancer immunotherapy. *Nat. Biomed. Eng.* **1**, 0011 (2017).
2. Conniot, J. et al. Immunization with mannosylated nanovaccines and inhibition of the immune-suppressing microenvironment sensitizes melanoma to immune checkpoint modulators. *Nat. Nanotechnol.* **14**, 891–901 (2019).
3. Sharma, P. & Allison, J. P. The future of immune checkpoint therapy. *Science* **348**, 56–61 (2015).
4. Ribas, A. & Wolchok, J. D. Cancer immunotherapy using checkpoint blockade. *Science* **359**, 1350–1355 (2018).
5. Waldman, A. D., Fritz, J. M. & Lenardo, M. J. A guide to cancer immunotherapy: from T cell basic science to clinical practice. *Nat. Rev. Immunol.* **20**, 651–668 (2020).
6. van Weverwijk, A. & de Visser, K. E. Mechanisms driving the immunoregulatory function of cancer cells. *Nat. Rev. Cancer* **23**, 193–215 (2023).
7. Robert, C. et al. Pembrolizumab versus ipilimumab in advanced melanoma. *N. Engl. J. Med.* **372**, 2521–2532 (2015).
8. Postow, M. A. et al. Nivolumab and ipilimumab versus ipilimumab in untreated melanoma. *N. Engl. J. Med.* **372**, 2006–2017 (2015).
9. Larkin, J. et al. Combined nivolumab and ipilimumab or monotherapy in untreated melanoma. *N. Engl. J. Med.* **373**, 23–34 (2015).
10. Weber, J. S., Kähler, K. C. & Hauschild, A. Management of immune-related adverse events and kinetics of response with ipilimumab. *J. Clin. Oncol.* **30**, 2691–2697 (2012).

11. Boutros, C. et al. Safety profiles of anti-CTLA-4 and anti-PD-1 antibodies alone and in combination. *Nat. Rev. Clin. Oncol.* **13**, 473–486 (2016).
12. Stadtmauer, E. A. et al. CRISPR-engineered T cells in patients with refractory cancer. *Science* **367**, eaba7365 (2020).
13. Su, S. et al. CRISPR-Cas9 mediated efficient PD-1 disruption on human primary T cells from cancer patients. *Sci. Rep.* **6**, 1–14 (2016).
14. Topalian, S. L., Taube, J. M., Anders, R. A. & Pardoll, D. M. Mechanism-driven biomarkers to guide immune checkpoint blockade in cancer therapy. *Nat. Rev. Cancer* **16**, 275–287 (2016).
15. Lu, Y. et al. Safety and feasibility of CRISPR-edited T cells in patients with refractory non-small-cell lung cancer. *Nat. Med.* **26**, 732–740 (2020).
16. Lacey, S. F. & Fraietta, J. A. First Trial of CRISPR-Edited T cells in Lung Cancer. *Trends Mol. Med.* **26**, 713–715 (2020).
17. Rupp, L. J. et al. CRISPR/Cas9-mediated PD-1 disruption enhances anti-tumor efficacy of human chimeric antigen receptor T cells. *Sci. Rep.* **7**, 1–10 (2017).
18. Labanieh, L., Majzner, R. G. & Mackall, C. L. Programming CAR-T cells to kill cancer. *Nat. Biomed. Eng.* **2**, 377–391 (2018).
19. Grosskopf, A. K. et al. Delivery of CAR-T cells in a transient injectable stimulatory hydrogel niche improves treatment of solid tumors. *Sci. Adv.* **8**, eabn8264 (2022).
20. Koehl, U. et al. Advances in clinical NK cell studies: donor selection, manufacturing and quality control. *Oncoimmunology* **5**, e1115178 (2016).
21. Elsallab, M. & Maus, M. V. Expanding access to CAR T cell therapies through local manufacturing. *Nat. Biotechnol.* **41**, 1698–1708 (2023).
22. Kranjc, M. & Miklavčič, D. Electric field distribution and electroporation threshold. *Handbook of Electroporation*, **2**, 1043–1058 (2016).
23. Jenkins, E. P. et al. Electrotherapies for glioblastoma. *Adv. Sci.* **8**, 2100978 (2021).
24. Sharpe, A. H. & Pauken, K. E. The diverse functions of the PD1 inhibitory pathway. *Nat. Rev. Immunol.* **18**, 153–167 (2018).
25. Chang, H. et al. Cryomicroneedles for transdermal cell delivery. *Nat. Biomed. Eng.* **5**, 1008–1018 (2021).
26. Eusébio, D. et al. Methods to improve the immunogenicity of plasmid DNA vaccines. *Drug Discov. Today* **26**, 2575–2592 (2021).
27. Bergman, P. et al. Development of a xenogeneic DNA vaccine program for canine malignant melanoma at the Animal Medical Center. *Vaccine* **24**, 4582–4585 (2006).
28. Ferraro, B. et al. Clinical applications of DNA vaccines: current progress. *Clin. Infect. Dis.* **53**, 296–302 (2011).
29. MacGregor, R. R. et al. First human trial of a DNA-based vaccine for treatment of human immunodeficiency virus type 1 infection: safety and host response. *J. Infect. Dis.* **178**, 92–100 (1998).
30. Xu, J. et al. A general strategy towards personalized nanovaccines based on fluoropolymers for post-surgical cancer immunotherapy. *Nat. Nanotechnol.* **15**, 1043–1052 (2020).
31. Baaten, B. J., Tinoco, R., Chen, A. T. & Bradley, L. M. Regulation of antigen-experienced T cells: lessons from the quintessential memory marker CD44. *Front. Immunol.* **3**, 23 (2012).
32. Twyman-Saint Victor, C. et al. Radiation and dual checkpoint blockade activate non-redundant immune mechanisms in cancer. *Nature* **520**, 373–377 (2015).
33. Wherry, E. J. & Kurachi, M. Molecular and cellular insights into T cell exhaustion. *Nat. Rev. Immunol.* **15**, 486–499 (2015).
34. Stephan, S. B. et al. Biopolymer implants enhance the efficacy of adoptive T-cell therapy. *Nat. Nanotechnol.* **33**, 97–101 (2015).
35. Fan, Q. et al. An implantable blood clot–based immune niche for enhanced cancer vaccination. *Sci. Adv.* **6**, eabb4639 (2020).
36. Boukany, P. E. et al. Nanochannel electroporation delivers precise amounts of biomolecules into living cells. *Nat. Nanotechnol.* **6**, 747–754 (2011).
37. Gallego-Pérez, D. et al. Topical tissue nano-transfection mediates non-viral stroma reprogramming and rescue. *Nat. Nanotechnol.* **12**, 974–979 (2017).
38. Mirvakili, S. M. & Langer, R. Wireless on-demand drug delivery. *Nat. Electron.* **4**, 464–477 (2021).
39. Wang, Y. et al. Transdermal microarrayed electroporation for enhanced cancer immunotherapy based on DNA vaccination. *Proc. Nat. Acad. Sci. USA* **121**, e2322264121 (2024).
40. Billingsley, M. M. et al. Orthogonal Design of Experiments for optimization of lipid nanoparticles for mRNA engineering of CAR T cells. *Nano Lett.* **22**, 533–542 (2021).
41. Huang, D. et al. Efficient delivery of nucleic acid molecules into skin by combined use of microneedle roller and flexible interdigitated electroporation array. *Theranostics* **8**, 2361–2376 (2018).
42. McKee, C. T., Last, J. A., Russell, P. & Murphy, C. J. Indentation versus tensile measurements of Young's modulus for soft biological tissues. *Tissue Eng. Part B Rev.* **17**, 155–164 (2011).
43. Yu, J. et al. Glucose-responsive insulin patch for the regulation of blood glucose in mice and minipigs. *Nat. Biomed. Eng.* **4**, 499–506 (2020).
44. Cheng, S. et al. Electronic Blood Vessel. *Matter* **3**, 1664–1684 (2020).
45. Dong, Z. & Chang, L. Recent electroporation-based systems for intracellular molecule delivery. *Nanotechnol. Precis. Eng.* **4**, 045001 (2021).
46. Garside, P. et al. Visualization of specific B and T lymphocyte interactions in the lymph node. *Science* **281**, 96–99 (1998).
47. De Castro, V., Galaine, J., Loyon, R. & Godet, Y. CRISPR-Cas gene knockouts to optimize engineered T cells for cancer immunotherapy. *Cancer Gene Ther.* **31**, 1124–1134 (2024).
48. Nguyen, L. T. & Ohashi, P. S. Clinical blockade of PD1 and LAG3–potential mechanisms of action. *Nat. Rev. Immunol.* **15**, 45–56 (2015).
49. Thibult, M.-L. et al. PD-1 is a novel regulator of human B-cell activation. *Int. Immunol.* **25**, 129–137 (2013)
50. Parayath, N., Stephan, S., Koehne, A., Nelson, P. & Stephan, M. In vitro-transcribed antigen receptor mRNA nanocarriers for transient expression in circulating T cells in vivo. *Nat. Commun.* **11**, 1–17 (2020).
51. Rurik, J. G. et al. CAR T cells produced in vivo to treat cardiac injury. *Science* **375**, 91–96 (2022).
52. Mardiana, S., Solomon, B. J., Darcy, P. K. & Beavis, P. A. Supercharging adoptive T cell therapy to overcome solid tumor–induced immunosuppression. *Sci. Transl. Med.* **11**, eaaw2293 (2019).
53. Rosell, R., Filipska, M., Chaib, I., Llige, D. & Laguia, F. Commentary: safety and feasibility of CRISPR-edited T cells in patients with refractory non-small-cell lung cancer. *Front. Oncol.* **10**, 1726 (2020).
54. Wang, C., Ye, Y., Hochu, G. M., Sadeghifar, H. & Gu, Z. Enhanced cancer immunotherapy by microneedle patch-assisted delivery of anti-PD1 antibody. *Nano Lett.* **16**, 2334–2340 (2016).
55. Shang, Q. et al. Rational design of a robust antibody-like small-molecule inhibitor nanoplatform for enhanced photo-immunotherapy. *Acs Appl. Mater. Inter.* **12**, 40085–40093 (2020).
56. Bois, H. D., Heim, T. A. & Lund, A. W. Tumor-draining lymph nodes: at the crossroads of metastasis and immunity. *Sci. Immunol.* **6**, eabg3551 (2021).
57. Francis, D. M. et al. Blockade of immune checkpoints in lymph nodes through locoregional delivery augmentscancer immunotherapy. *Sci. Transl. Med.* **12**, eaay3575 (2020).
58. June, C. H., O'Connor, R. S., Kawalekar, O. U., Ghassemi, S. & Milone, M. C. CAR T cell immunotherapy for human cancer. *Science* **359**, 1361–1365 (2018).

59. Hendel, A. et al. Chemically modified guide RNAs enhance CRISPR-Cas genome editing in human primary cells. *Nat. Biotechnol.* **33**, 985–989 (2015).
60. Ren, J. et al. Multiplex genome editing to generate universal CAR T cells resistant to PD1 inhibition. *Clin. Cancer Res.* **23**, 2255–2266 (2017).
61. Kim, S., Kim, D., Cho, S. W., Kim, J. & Kim, J.-S. Highly efficient RNA-guided genome editing in human cells via delivery of purified Cas9 ribonucleoproteins. *Genome Res.* **24**, 1012–1019 (2014).
62. Wang, H. X. et al. CRISPR/Cas9-based genome editing for disease modeling and therapy: challenges and opportunities for nonviral delivery. *Chem. Rev.* **117**, 9874–9906 (2017).
63. Miyamoto, K. et al. Direct in vivo reprogramming with Sendai virus vectors improves cardiac function after myocardial infarction. *Cell Stem Cell* **22**, 91–103.e105 (2018).
64. Kurita, M. et al. In vivo reprogramming of wound-resident cells generates skin epithelial tissue. *Nature* **561**, 243–247 (2018).
65. Kaemmerer, E. et al. Gelatine methacrylamide-based hydrogels: an alternative three-dimensional cancer cell culture system. *Acta Biomater.* **10**, 2551–2562 (2014).

Acknowledgements

This work was supported by National Natural Science Foundation of China (U20A20194, P.S, 32201176, 32471464, Z.W.), by General Research Fund (11215920, 11220024, 11218522, 11218523, P.S.) from the Research Grants Council of Hong Kong SAR, and Shenzhen-Hong Kong-Macau Science and Technology Program (Category C, SGDX2020110309300502, P.S.). Support from Innovation and Technology Commission of Hong Kong through the Centre for Cerebro-Cardiovascular Health Engineering and funds from City University of Hong Kong (7005084, 7005206, 7005642, 7020003, 7020077, 9680233, 9240060, P.S.) are also acknowledged.

Author contributions

P.S. supervised the research. P.S., J.Q., and Y.W. conceived the project, designed the experiments. J.Q. and Y.W. performed the experiments and analyzed the data. C.X., M.W., X.H., W.J., and Z.W. contributed to the experimental work. C.Y.L. and B.Y.K. contributed to the DNA synthesis. T.Z. and W.L. contributed to the animal related experiments. J.Q., Y.W., and P.S. wrote the manuscript, and other authors also contributed to the writing of the manuscript.

Competing interests

The authors declare the following competing interests: P.S., J.Q., Y.W., and X.H. are listed as inventors on a patent application, titled "Micro-electroporation based drug delivery system, methods for use and fabrication thereof" (US Priority No. 17/804,118), filed by the City University of Hong Kong. The other authors declare no competing interests.

Additional information

Supplementary information The online version contains supplementary material available at https://doi.org/10.1038/s41467-024-54292-0.

Correspondence and requests for materials should be addressed to Peng Shi.

Peer review information *Nature Communications* thanks Grégory Verdeil and the other, anonymous, reviewer(s) for their contribution to the peer review of this work. A peer review file is available.